
VITA: VISION-TO-ACTION FLOW MATCHING POLICY

Dechen Gao¹, Boqi Zhao¹, Andrew Lee¹, Ian Chuang², Hanchu Zhou³, Hang Wang³,

Zhe Zhao¹, Junshan Zhang³, Iman Soltani⁴

¹Department of Computer Science, University of California, Davis

²Department of Electrical Engineering and Computer Sciences, University of California, Berkeley

³Department of Electrical and Computer Engineering, University of California, Davis

⁴Department of Mechanical and Aerospace Engineering, University of California, Davis
dchgao@ucdavis.edu, boqzhao@ucdavis.edu, awclee@ucdavis.edu, ianc@berkeley.edu
hczhou@ucdavis.edu, whang@ucdavis.edu, zao@ucdavis.edu, jzh@ucdavis.edu,
isoltani@ucdavis.edu

October 3, 2025

ABSTRACT

Conventional flow matching and diffusion-based policies sample through iterative denoising from standard noise distributions (e.g., Gaussian), and require conditioning mechanisms to incorporate visual information during the generative process, incurring substantial time and memory overhead. To reduce the complexity, we develop VITA (**V**ision-**T**o-**A**ction policy), a *noise-free* and *conditioning-free* policy learning framework that directly maps visual representations to latent actions using flow matching. VITA treats latent visual representations as the source of the flow, thus eliminating the need of conditioning. As expected, bridging vision and action is challenging, because actions are lower-dimensional, less structured, and sparser than visual representations; moreover, flow matching requires the source and target to have the same dimensionality. To overcome this, we introduce an action autoencoder that maps raw actions into a structured latent space aligned with visual latents, trained jointly with flow matching. To further prevent latent space collapse, we propose flow latent decoding, which anchors the latent generation process by backpropagating the action reconstruction loss through the flow matching ODE (ordinary differential equations) solving steps. We evaluate VITA on 8 simulation and 2 real-world tasks from ALOHA and Robomimic. VITA outperforms or matches state-of-the-art generative policies, while achieving $1.5\times$ - $2.3\times$ faster inference compared to conventional methods with conditioning. Project page: [VITA](#).

Keywords Imitation Learning · Flow Matching · Robotics Manipulation · Policy Learning

1 Introduction

Flow matching and diffusion models have demonstrated remarkable success across a wide range of cross-modal generation tasks, from text-to-image generation [1, 2, 3, 4, 5, 6], text-to-video generation [7, 8, 9], to visuomotor (vision-to-action) policy [10, 11, 12, 13, 14, 15, 16, 17]. Conventional flow matching and diffusion methods [18, 19] generate samples by starting with noise sampled from a basic source distribution (often Gaussian) and progressively “denoising” them into the target modality, requiring additional conditioning mechanisms [1, 6, 10, 20] to inject visual modality at denoising steps, which incurs increased time and space complexity [4, 5].

Clearly, minimizing complexity is critical for effective real-time robot control. To overcome the inefficiencies inherent to conditioning mechanisms in conventional methods, we develop VITA (**V**ision-**T**o-**A**ction flow matching), a noise-free policy learning framework that directly maps visual representations to latent actions. As depicted in Figure 1, unlike conventional methods that flow from a Gaussian prior and inject visual contexts via conditioning mechanisms during

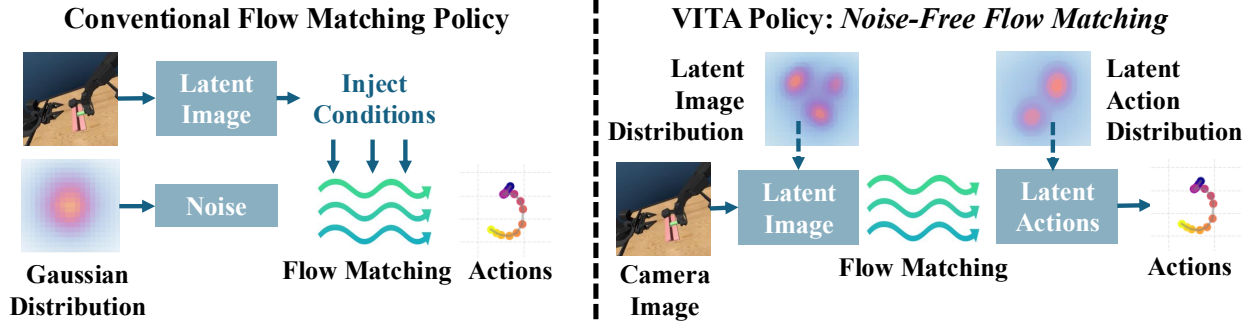


Figure 1: A comparison between VITA and conventional flow matching and diffusion policies. Unlike conventional methods that sample noise from standard distributions and inject source input modalities via conditioning during generation, VITA poses no constraints on the source distributions, and flow directly from latent visual representations to latent actions, eliminating the need for conditioning.

generation, VITA poses no constraints on the source distribution, and directly flows from latent visual representations, obviating the need for injecting visual inputs via conditioning modules. Consequently, VITA significantly reduces inference latency and memory overhead, simplifying the network architecture.

Learning vision-to-action flow matching, however, presents several new challenges. In general, bridging two distinct modalities is inherently difficult [4, 5], particularly in robot learning where action data is relatively limited, unstructured and sparse, whereas the visual representations exhibit rich structures and semantics and have far higher dimensions. Additionally, flow matching requires that the source and target have equal dimensionalities, which prevents directly pairing raw actions with visual representations.

To address these challenges, we propose two key designs for VITA. 1) **Learned target latent actions for flow matching.** We introduce a structured latent action space, learned via an action autoencoder, that ‘lifts’ action representations to match the higher dimensionality of visual representations and serves as a structured target distribution for flow matching. The action encoder up-samples raw actions into target latent actions, and a decoder reconstructs raw actions from these latents. 2) **Flow latent decoding.** In conventional flow matching methods such as latent diffusion for image generation [1], the target latent space can be pre-trained with abundant image data and then frozen as reliable flow matching targets; in contrast, we show that a pre-trained and frozen latent action space for learning vision-to-action flows yields poor performance, since action data can be too sparse and limited to learn reliable target latents and frozen latent spaces cannot be corrected. It is therefore plausible to jointly train the flow model with the action autoencoder. To prevent model collapse of target latent action space (which happens by naively reducing the flow matching and autoencoder loss), we introduce flow latent decoding which backpropagates the reconstruction loss of latent actions generated by solving flow matching ordinary differential equations (ODE), anchoring the latent generation process using ground-truth actions. This approach also bridges the *training-inference gap of latent actions*: during training, the flow matching model learns to match the targets given by the action encoder, and the decoder is trained to reconstruct these targets. whereas at test time, the decoder must reconstruct ODE-generated latent actions.

We evaluate VITA on both real-world and simulated tasks using ALOHA [21, 22, 23] and Robomimic [24]. Our experiments demonstrate that VITA outperforms or matches state-of-the-art generative policies. We implement VITA with only MLP layers. Compared to state-of-the-art flow matching and diffusion policies that predominantly leverage complex architecture such as transformers [3] or U-Net [25], and introduce conditioning modules [26, 14], the MLP-only and noise-free VITA policy achieves, $1.5\times$ - $2.3\times$ faster inference compared to conventional flow matching. To our knowledge, VITA is the first MLP-only flow matching policy to succeed on tasks as challenging as ALOHA bi-manual manipulation.

Our main contributions are summarized as follows:

Noise-Free Flow Matching for Visuomotor Learning. We propose VITA, a noise-free policy that directly evolves latent visual representations into latent actions via flow matching. To bridge the modality gap, VITA incorporates an action autoencoder that maps raw actions into structured latent spaces aligned with visual representations. To prevent latent space collapse, we propose flow latent decoding, which anchors latent generation using ground-truth actions by backpropagating the action reconstruction loss through the flow matching ODE (ordinary differential equations) solving steps.

An Efficient Policy Architecture. By treating vision as the source distribution, VITA obviates costly conditioning mechanisms required by conventional diffusion and flow matching policies. VITA also enables a lightweight MLP-only

implementation that achieves superior performance on challenging bi-manual manipulation tasks with high-dimensional visual inputs.

State-of-the-Art Performance in Real and Simulated Environments. We validate VITA’s effectiveness on 8 simulation and 2 real-world tasks. VITA surpasses or matches state-of-the-art generative policies in success rates while delivering $1.5\times-2.3\times$ faster inference compared to conventional flow matching approaches.

2 Related Work

Imitation Learning for Visuomotor Policy. Imitation learning enables robots to learn complex behaviors by mimicking expert demonstrations. Behavior cloning is a prominent imitation learning paradigm that learns a policy that maps observations to actions [26, 27] via supervised learning. Recent advancements in behavioral cloning have widely adopted autoregressive modeling [28, 29, 13] and generative modeling [10]. Generative modeling learns a conditional distribution of actions given an observation, leveraging conditional variational autoencoders (CVAEs) [26, 27], diffusion [20, 10], or flow matching [30, 14]. Generative models ubiquitously require conditioning modules (e.g., cross-attention [20], AdaLN [20], FiLM [31, 10]) to inject observations at each step of the generation process. VITA removes the visual conditioning module by developing a noise-free and conditioning-free vision-to-action flow.

Diffusion and Flow matching for Generative Modeling. Diffusion and flow matching models have shown strong performance across diverse generative tasks, such as image and video generation [1, 7], and visuomotor policies [10]. Unlike diffusion which samples from a Gaussian distributions, flow matching theoretically places no constraints on the choice of source distribution [32]. A few works have explored this property to learn the direct transport within the same modality [33, 34]. Recently, [4] and [5] extended this to more challenging cross-modal generation between text and image. VITA focuses on learning to bridge vision and action for visuomotor control, where the action modality presents unique challenges because of limited data and its unstructured nature. Different from flow matching for image generation, which typically pre-trains and freezes the latent image space when learning the flow [1, 5, 4], VITA resorts to a fully end-to-end pipeline training to effectively learn the latent action space from limited and sparse action data along with flow matching. We propose flow latent decoding to backpropagate action reconstruction losses through the the latent action generation process (ODE solving steps) during training.

3 Preliminaries

Flow matching models learn to transport samples from a source probability distribution p_0 to a target distribution p_1 by learning a velocity vector field v_θ [18, 35]. This generative process is defined by an ordinary differential equation (ODE), $\frac{dz_t}{dt} = v_\theta(z_t, t)$, where $t \in [0, 1]$ is a continuous time variable, z_t represents a sample at time t , and the model v_θ is a neural network. The goal of training is for v_θ to generate a path that transforms a sample $z_0 \sim p_0$ into a corresponding sample $z_1 \sim p_1$.

For a simple, straight probability path between two samples, the interpolated state at time t is defined as $z_t = (1-t)z_0 + tz_1$. The corresponding ground-truth velocity of this path given by $u_t = \frac{dz_t}{dt} = z_1 - z_0$. The network v_θ is trained by minimizing the Mean Squared Error (MSE) between its predicted velocity and the ground-truth velocity:

$$\mathcal{L}_{\text{FM}} = \mathbb{E}_{t, z_0, z_1} \left[\|v_\theta(z_t, t) - (z_1 - z_0)\|^2 \right] \quad (1)$$

During inference, starting from a source sample z_0 , the model generates a target sample \hat{z}_1 by solving the ODE initial value problem from $t = 0$ to $t = 1$:

$$\hat{z}_1 = z_0 + \int_0^1 v_\theta(z_t, t) dt \quad (2)$$

Notably, conventional flow matching or diffusion policies for visuomotor control generate actions by evolving a sample from a simple prior distribution, such as Gaussian noise ($z_0 \sim \mathcal{N}(0, I)$), and require conditioning on visual inputs to guide the generation process [30, 10, 20]. However, flow matching does not assume the source distribution must be simple noise; it can theoretically connect two arbitrary distributions. We exploit this flexibility to re-formulate generative visuomotor policy learning: we directly use the latent distribution of visual observations as the source distribution p_0 , yielding a noise-free flow matching process that eliminates the need for costly conditioning modules and therefore boosts time and space efficiency.

4 VITA: Vision-to-Action Flow Matching

The key challenge in VITA is the large dimensionality gap between vision and action, compounded by the sparsity and unstructured nature of action data. In this section, we present the core designs of VITA developed to address these issues. We first introduce the mathematical formulation of VITA (Section 4.1) and its overall architecture (Section 4.2). We then show why constructing a latent action space is essential for resolving dimensionality mismatch (Section 4.3), and propose flow latent decoding to address model collapse. Finally, we describe the objectives that enable effective end-to-end VITA learning from scratch (Section 4.4).

4.1 Flowing from Vision to Action

VITA learns a policy $\pi(A|O)$ that directly maps observations O to a corresponding sequence of future actions A . The observations O encompasses raw visual inputs $I \in \mathbb{R}^{H \times W \times C}$ and, optionally, the robot’s proprioceptive state vector S . Actions are represented as temporal sequences over a prediction horizon, formally defined as $A \in \mathbb{R}^{T_{\text{pred}} \times D_{\text{action}}}$, where T_{pred} is the prediction horizon and D_{action} is the dimensionality of the action space. We employ action chunking with $T_{\text{pred}} > 1$ to enhance temporal consistency [26].

Unlike conventional flow matching policies that generate actions through conditional denoising of random noise given visual inputs, VITA formulates the visuomotor policy as an unconditional flow between the source distribution of latent visual representations p_0 and the target distribution of latent actions p_1 . The flow matching framework learns to evolve a latent visual representation z_0 into an latent action representation z_1 by learning a velocity field $v_\theta(z_t, t)$, where $t \in [0, 1]$ represents the continuous time parameter interpolating between the source state at $t = 0$ and the target state at $t = 1$. Critically, flow matching requires z_0 and z_1 to share identical dimensionality, necessitating the construction of a latent action space that matches the dimensionality of visual representations (Section 4.3).

During inference, the current observation O_{curr} is first encoded into its latent visual representation $z_0 = \mathcal{E}_v(O_{\text{curr}})$. This latent vector is subsequently evolved into a predicted action latent representation, \hat{z}_1 , by numerically solving the ODE from $t = 0$ to $t = 1$ using the learned velocity field v_θ : $\hat{z}_1 = z_0 + \int_0^1 v_\theta(z_t, t) dt$. In other words, \hat{z}_1 is obtained by numerically solving the flow matching ODE, and serves as an approximation to the target latent z_1 . The resulting latent action vector \hat{z}_1 is then decoded through the action decoder to yield the final action sequence $\hat{A} = \mathcal{D}_a(\hat{z}_1)$.

4.2 VITA Architecture Design

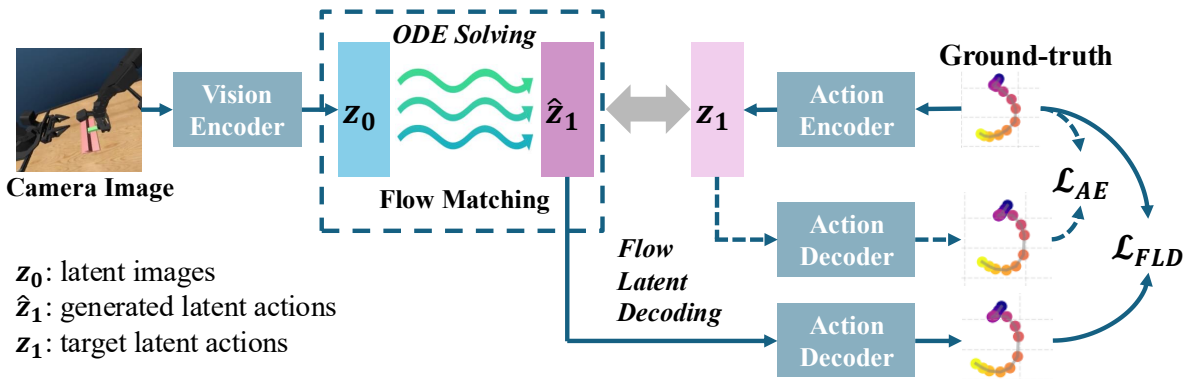


Figure 2: An overview of the VITA architecture: The vision encoder maps observations into a source latent representation z_0 for the flow; the action encoder provides a target latent representation z_1 for flow matching. The action decoder learns to decode \hat{z}_1 (latent actions generated by solving ODEs) to actions via flow latent decoding losses, and decode z_1 to actions (latent actions from action encoder) via AE losses. The flow matching network is designed to learn the velocity field over a continuous flow matching path from z_0 to \hat{z}_1 .

As depicted in Figure 2, VITA is composed of the three primary components: 1) The **Vision Encoder** (\mathcal{E}_v) maps raw camera images into a vector representation of visual latents I . The observation O to the policy consists of both image vector representations I and, optionally, the robot’s proprioceptive states S . In short, O is mapped into a latent vector $z_0 = \mathcal{E}_v(O)$, where $z_0 \in \mathbb{R}^{D_{\text{latent}}}$ is the source of flow matching. 2) The **Action Autoencoder (AE)** consists of the Action Encoder and the Action Decoder, and learns a compact representation for action chunks. The Action Encoder (\mathcal{E}_a) maps the ground-truth action chunk A to latent actions $z_1 = \mathcal{E}_a(A)$, where $z_1 \in \mathbb{R}^{D_{\text{latent}}}$ serves as the target for

flow matching; the Action Decoder (\mathcal{D}_a) reconstructs an action chunk $\hat{A} = \mathcal{D}_a(\hat{z}_1)$ from latent actions \hat{z}_1 . 3) The **Flow Matching Network** (v_θ) is learned to predict the velocity field at arbitrary t .

4.3 Bridging the Modality Gap between Vision and Action

A key constraint of flow matching is that the source and target distributions must share the same dimensionality. This poses a critical challenge for vision-to-action policies, since action spaces are typically much lower-dimensional than visual representations. For example, action dimensionalities range from 2 on PushT to 21 on ThreadNeedle, whereas visual representations can be 512-dimensional [23] or even higher when using grid-based tokenizers [10].

To bridge the gap, one naive option is to down-sample latent visual representations to action chunk dimensionalities which, however, causes severe information loss and degrades performance. Alternatively, one can up-sample actions with zero-padding, yielding sparse, unstructured targets that hinder flow matching learning (see Appendix B.1). A third alternative is a pre-trained, frozen action AE, akin to common practice in latent diffusion for image generation [1], but this proves ineffective for learning vision-to-action flow: with sparse, limited action data the induced latent space is unreliable as a flow target and cannot be corrected once frozen. As another alternative, jointly training the action AE with flow matching may still fail, and our empirical studies identify the root cause as latent space collapse induced by a training-inference gap in the latent actions used for decoding as detailed below.

Training-Inference Gap between Encoder-Based and ODE-Generated Latent Actions. During training, the decoder reconstructs actions from encoder-based latent actions z_1 , whereas at inference it decodes \hat{z}_1 generated by solving the flow matching ODE. Since \hat{z}_1 is an approximation, and does not always align with z_1 , the decoder can fail to map them into meaningful actions. To address this gap, we propose flow latent decoding, which enforces the model to decode from ODE-generated latent actions \hat{z}_1 during training, anchoring the latent generation process with ground-truth actions.

4.4 VITA Learning Objectives

Building upon our analysis of the training-inference gap, we now formulate a comprehensive learning framework for VITA that prevents latent collapse while ensuring effective end-to-end optimization. Our framework includes three essential objectives: flow latent decoding (FLD), flow matching (FM), and action autoencoder (AE) losses, each addressing distinct aspects of the learning challenge.

Flow Latent Decoding (FLD). FLD addresses the training-inference gap by anchoring ODE-generated actions using ground-truth actions during training. Formally, FLD is defined as the reconstruction loss using ODE-generated latent actions, $\mathcal{L}_{\text{FLD}} = \|\mathcal{D}_a(\hat{z}_1) - A\|$, where \hat{z}_1 is obtained by solving the flow ODE with an Euler solver during training. FLD propagates gradients through the decoder and the ODE solver into both v_θ and \mathcal{E}_v . By decoding \hat{z}_1 into actions and measuring reconstruction error directly in action space, FLD effectively minimizes the discrepancies between encoder-based and ODE-generated latents.

Flow Latent Consistency (FLC). To gain deeper insight into the mechanics of FLD, we introduce flow latent consistency (FLC), a minimalist surrogate that directly aligns ODE-generated and encoder-based latents without decoding. Formally, FLC is defined as $\mathcal{L}_{\text{FLC}} = \|\hat{z}_1 - z_1\|$. Under mild local regularity assumptions on \mathcal{D}_a (stated below), FLC and FLD provide locally equivalent training signals for the same \hat{z}_1 . Empirically, FLC also prevents collapse without explicit action reconstruction, though convergence is slightly slower than with FLD (Section 5.3). This theoretical connection not only validates our approach but also offers computational flexibility in implementation. A sketch of the analysis is given below, with full proofs and corollaries deferred to Appendix A.

Assumption 1 (Decoder locally well-behaved). \mathcal{D}_a is C^1 in a neighborhood of z_1 , with Jacobian singular values bounded as $m \leq \sigma_{\min} \leq \sigma_{\max} \leq L$ on that neighborhood. Let $\varepsilon_{\text{AE}} := \|\mathcal{D}_a(z_1) - A\|$ denote the local AE reconstruction error.

Theorem 1 (Local equivalence of FLD and FLC). Under ?? 1, for any \hat{z}_1 in the neighborhood,

$$m \|\hat{z}_1 - z_1\| - \varepsilon_{\text{AE}} \leq \|\mathcal{D}_a(\hat{z}_1) - A\| \leq L \|\hat{z}_1 - z_1\| + \varepsilon_{\text{AE}}.$$

If $\varepsilon_{\text{AE}} = 0$, the minimizers of \mathcal{L}_{FLD} and \mathcal{L}_{FLC} coincide and equal $\{z_1\}$; if $\varepsilon_{\text{AE}} > 0$, any minimizer of \mathcal{L}_{FLD} lies within radius $\varepsilon_{\text{AE}}/m$ of z_1 .

This theoretical result confirms that FLD and FLC target the same underlying optimization objective.

We will provide further discussion in Section 5.3, showing that including the flow latent decoding loss with a non-zero λ_{FLD} is critical for avoiding latent space collapse and training successful VITA policies. We will also ablate the effects of λ_{FLD} , λ_{FLC} , and λ_{AE} in Figure 6.

Flow Matching and Autoencoder Losses. The flow matching loss supervises the flow network v_θ by minimizing the MSE between the predicted velocity and the ground-truth velocity as shown in Equation (1). The action autoencoder loss trains $(\mathcal{E}_a, \mathcal{D}_a)$ to reconstruct action chunks using an L1 loss, $\mathcal{L}_{\text{AE}} = \|A - \mathcal{D}_a(\mathcal{E}_a(A))\|_1$, where $z_1 = \mathcal{E}_a(A)$ serves as a structured target latent with small reconstruction bias and good local conditioning. This structured latent space strengthens the theoretical link between FLD and FLC and further stabilizes training.

The training objective can be written as a weighted sum of all three losses: $\mathcal{L}_{\text{VITA}} = \lambda_{\text{FM}}\mathcal{L}_{\text{FM}} + \lambda_{\text{FLD}}\mathcal{L}_{\text{FLD}} + \lambda_{\text{AE}}\mathcal{L}_{\text{AE}}$.

5 Experiments

We evaluate VITA on ALOHA [21, 22] across 5 simulation tasks (Figure 3) and 2 real-world tasks (Figure 4). The simulation environments and datasets are from AV-ALOHA [21], which extend ALOHA with an additional 7-DoF arm equipped with an active-vision camera that dynamically adjusts its viewpoint. This setup increases task difficulty due to the larger action space and non-stationary observation dynamics. In addition, we evaluate on 2 single-arm Robomimic simulation tasks.

For simulation tasks, each environment provides 100-200 demonstrations. Demonstrations were collected from human experts in simulation using VR headsets, with the left-eye image used as input. VITA was trained at 25/3 FPS on AV-ALOHA and 20 FPS on Robomimic. For real-world tasks on AV-ALOHA, (Figure 4). Each task is trained with 50 demonstrations, using the left image from the stereo active-vision camera as input. VITA was trained at 11 FPS, and linearly interpolated to 33 FPS for deployment on the physical robot.

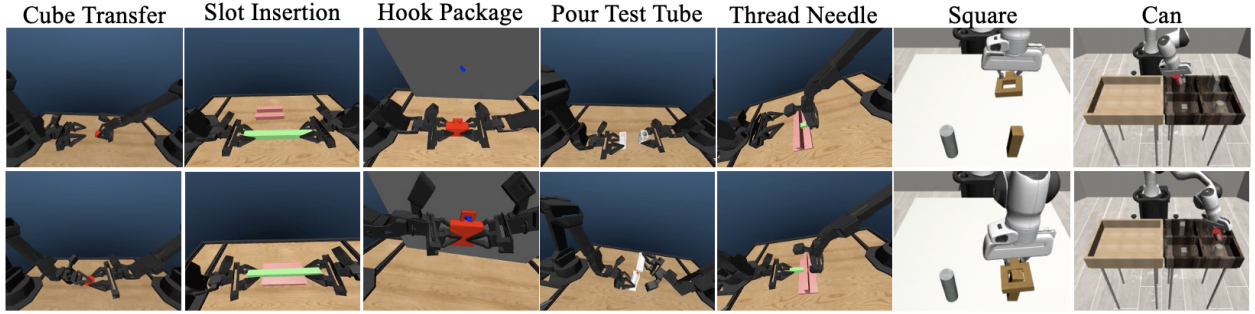


Figure 3: An illustration of 5 AV-ALOHA tasks (CubeTransfer, SlotInsertion, HookPackage, PourTestTube, ThreadNeedle), and 2 Robomimic tasks (Square, Can).

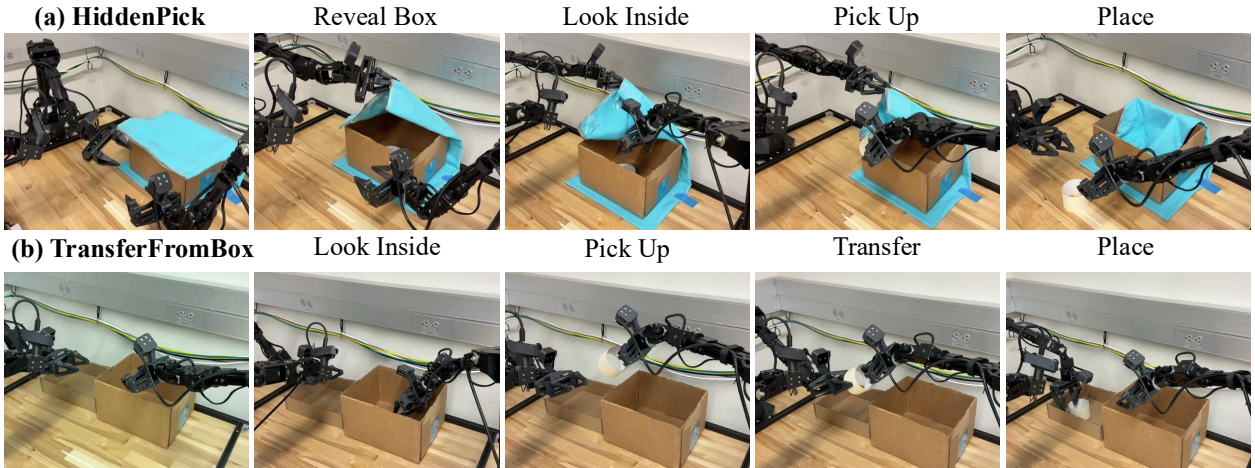


Figure 4: An illustration of two challenging real-world AV-ALOHA tasks, HiddenPick, and TransferFromBox. The pictures are taken from autonomous rollouts by the VITA policy.

5.1 Implementation

Flow Matcher. We adopt OT-CFM [36], a conditional flow matching method based on optimal transport, and solve the Euler ODE with 6 steps using linearly interpolated t for both VITA and FM baselines.

Networks. We use the widely adopted ResNet-18 [37, 13, 10] as the vision encoder for all the experiments. We use the 512-dimensional feature vector after the average pooling layer as the visual representations for VITA. Therefore, the source z_0 and target latents z_1 are both 512-dimensional vectors ($D_{\text{latent}} = 512$). The vector representations and conditioning-free design is amenable to simple and efficient implementation. For example, we use 4-layer MLP-only networks for both flow matching and decoding.

Training & Evaluation. We train VITA on each task for 50,000 steps with a batch size of 128. The policy predicts action chunks of length 16, of which the first 8 actions are executed. In simulation, we evaluate the policy every 500 steps, with each evaluation consisting of 50 episodes. We report the best success rates (SRs), averaged over 3 random seeds, for both VITA and baselines (Table 1). For real-world tasks, we evaluate 3 checkpoints over 20 episodes each and report the best SRs (Table 2).

Baselines. We compare VITA against state-of-the-art generative policies, including flow matching (FM) policy [30], diffusion policy (DP)[10], and action chunking transformer (ACT)[26]. We follow the ACT and DP implementation in LeRobot [38]. We found DP requires significantly more training steps than FM; ACT yields sub-optimal performance on most tasks; therefore, we increase training steps to 200,000 for both DP and ACT, and then report the best success rates. For DP, each inference takes 10 DDPM (Denosing Diffusion Probabilistic Model) steps [10]. We evaluate both the task performance and inference efficiency of VITA relative to these baselines in Section 5.2.

5.2 Performance

Success Rates. We evaluate VITA against state-of-the-art conditional generative policies on 8 simulated tasks: 5 bimanual AV-ALOHA tasks with active vision [21], 2 single-arm Robomimic tasks [24], and 1 PushT task. Results are reported in Table 1. Across all simulation tasks, VITA consistently outperforms or matches state-of-the-art baselines. ACT shows limited performance even after convergence, while DP requires significantly more training steps and remains sub-optimal despite extended training. We further assess VITA in real-world settings on two challenging AV-ALOHA tasks, with performance summarized in Table 2 and examples of autonomous rollouts in Figure 4, highlighting the precision of vision-to-action flow in manipulation tasks with high-dimensional visual inputs and large action spaces.

Table 1: Task success rates (SR) across simulation tasks including ALOHA, Robomimic, and PushT. We report the best SR during validation, and compute the mean across 3 random seeds.

Task	VITA	FM	DP	ACT
ThreadNeedle	0.92	0.88	0.00	0.52
SlotInsertion	0.76	0.83	0.20	0.50
PourTestTube	0.79	0.84	0.06	0.14
HookPackage	0.86	0.83	0.12	0.22
CubeTransfer	1.00	1.00	0.76	0.98
PushT	0.88	0.84	0.80	0.30
Square	1.00	1.00	1.00	0.46
Can	1.00	1.00	1.00	0.78

Table 2: Success rates of VITA on two real-world AV-ALOHA tasks. Each task has 3 subtasks.

Subtask	HiddenPick			TransferFromBox		
	Reveal	Pick	Place	Pick	Transfer	Place
SR	1.00	0.65	0.65	1.00	0.95	0.90

Efficiency. The VITA policy is highly efficient due to its architectural simplicity. The core components used during inference, the flow matching network and the action decoder, are both lightweight MLP-only networks. We use vector representations for both vision and action, further reducing time and space overhead. VITA contains 31M parameters, including the ResNet-18. We benchmark the inference latency and policy throughput of VITA and compare it against conventional flow matching policy baselines. We implement two different flow matching parameterizations, including diffusion transformer [2], and U-Net [25], and three different conditioning mechanisms, including AdaLN [2, 20],

cross-attention [39, 20, 29], and FiLM [31, 10], as the baselines. FM and DP are typically parameterized using U-Nets [25] or diffusion transformers (DiTs) [2], and are trained to predict velocity fields or noise at each denoising step. While U-Nets and DiTs are highly expressive, they can be large or computationally expensive, posing a drawback for real-world robotic deployments that require low-latency inference. Most importantly, these methods inevitably incorporate visual conditioning mechanisms, such as cross, further increasing both inference time and memory footprint.

With a control frequency of $25/3 \approx 8.33$ Hz, our MLP-only VITA policy achieves an inference wall-clock time of 0.22 ms on an NVIDIA 4090 GPU. In contrast, a comparable transformer-based flow matching policy incurs higher latency (0.33-0.51 ms) and requires more parameters. A detailed breakdown of efficiency metrics is given in Table 3.

Table 3: Model sizes and inference latency of different policy implementations.

Model	Conditioning	Architecture	Num of Params	Latency (ms/chunk)
VITA	N/A	MLP	31.09M	0.2215
FM	AdaLN	DiT	31.16M	0.3307
FM	Cross-Attn	DiT	29.06M	0.5102
FM	FiLM	U-Net	84.05M	0.3650
DDPM	FiLM	U-Net	81.82M	2.5985

5.3 Ablation of Flow Latent Decoding

We investigate the importance of flow latent decoding (\mathcal{L}_{FLD}) for effectively training VITA policies. During training, the decoder is trained by reconstructing from encoder-based latent actions z_1 , while during inference, the decoder needs to reconstruct from ODE-generated latent actions \hat{z}_1 . As a result, the generated latent actions at inference may not decode into meaningful actions, as demonstrated by Figure 5. To bridge this gap, we propose two objectives to minimize the discrepancy between encoder-based latents z_1 and ODE-generated latents \hat{z}_1 : (1) FLD, which decodes \hat{z}_1 into the action space and computes the reconstruction error against the ground-truth action; and (2) FLC, which directly aligns the predicted latent action with the encoded latent target $z_1 = \mathcal{E}_a(A)$ using $\|\hat{z}_1 - z_1\|$.

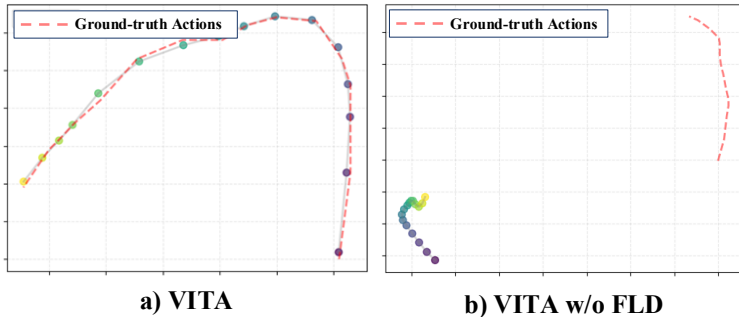


Figure 5: Comparison of reconstructed actions between (a) VITA, and (b) VITA without FLD. Reconstruction fails without FLD because of latent space collapse.

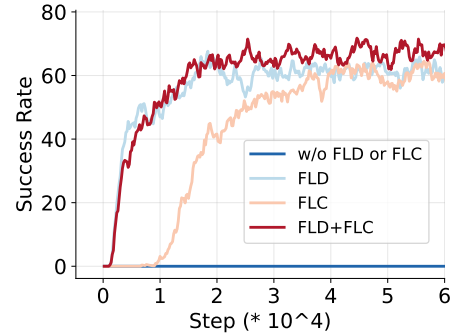


Figure 6: Success rates using different objectives.

As shown in Figure 6, without flow latent decoding (i.e., $\lambda_{\text{FLD}} = 0$), the model completely fails to learn a reasonable policy. In contrast, applying FLD succeeds in learning the policy. FLC provides a weaker signal compared to FLD (because FLD directly anchors using the ground-truth actions), resulting in slightly slower convergence. However, we found that using a combination of both objectives yields the best performance due to richer learning signals on both action space and latent space. In short, FLD and FLC are crucial for learning VITA, and in practice a combination of both can achieve optimal results.

5.4 VITA Denoising Process

Figure 7 compares the denoising processes of VITA and conventional flow matching. By jointly optimizing the vision-to-action flow and an action autoencoder with FLD, VITA induces highly structured latent spaces for both vision and action representations. As a result, even the latent image can be directly decoded into a coherent trajectory using the action decoder, which is then progressively refined by the VITA flow matching ODE.

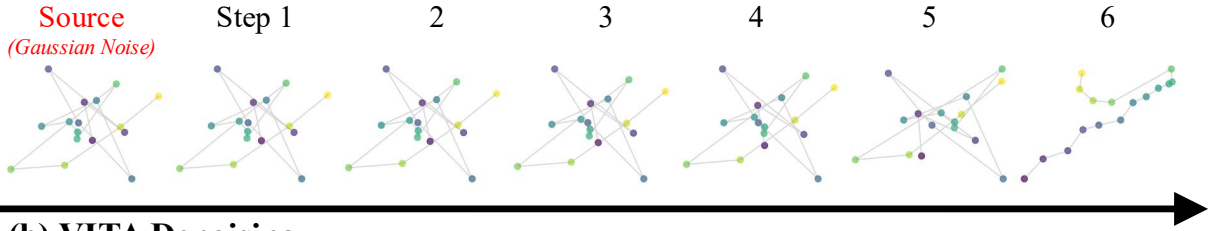
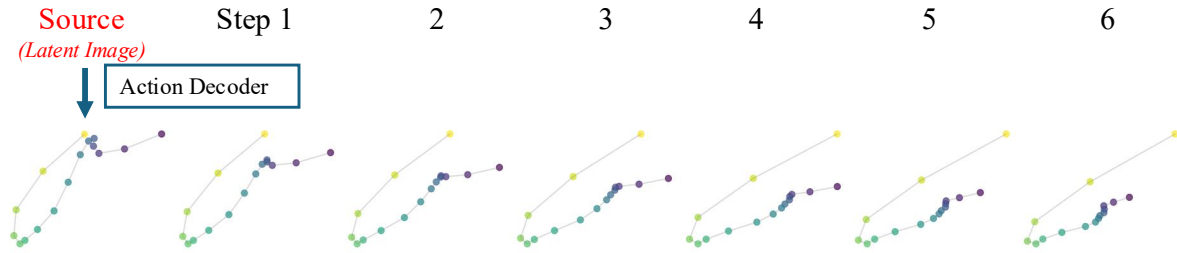
(a) Conventional Flow Matching Denoising**(b) VITA Denoising**

Figure 7: Conventional flow matching (a) flows from random Gaussian noise, and gradually “denoise” into raw action chunks by solving ODEs; in contrast, VITA (b) flows from latent images to latent actions, and the latent actions are then decoded to action chunks.

6 Conclusion

In this work, we developed VITA, an efficient and high-performing visuomotor policy. VITA generates actions in a noise-free manner and directly evolves latent visual representations into latent actions. By leveraging latent image representations as the flow’s source distribution, VITA eliminates the need for complex conditioning mechanisms such as cross-attention, significantly simplifying model architecture and enhancing efficiency. VITA employs vector representations for both latent images and actions, thereby enabling a simple MLP-only architecture for vision-to-action flow. Two key designs are critical to VITA’s success — structuring the latent action space using an action autoencoder and enabling backpropagation of flow latent decoding losses across ODE solving steps — allowing VITA to effectively learn latent action spaces with flow matching in a fully end-to-end manner. Extensive experiments demonstrate that VITA achieves state-of-the-art performance on ALOHA and Robomimic in both real and simulation tasks. VITA achieves $1.5\times$ – $2.3\times$ faster inference compared to conventional flow matching using different conditioning mechanisms.

References

- [1] Robin Rombach, Andreas Blattmann, Dominik Lorenz, Patrick Esser, and Björn Ommer. High-resolution image synthesis with latent diffusion models. In *Proceedings of the IEEE/CVF conference on computer vision and pattern recognition*, pages 10684–10695, 2022.
- [2] William Peebles and Saining Xie. Scalable diffusion models with transformers. In *Proceedings of the IEEE/CVF international conference on computer vision*, pages 4195–4205, 2023.
- [3] Nanye Ma, Mark Goldstein, Michael S Albergo, Nicholas M Boffi, Eric Vanden-Eijnden, and Saining Xie. Sit: Exploring flow and diffusion-based generative models with scalable interpolant transformers. In *European Conference on Computer Vision*, pages 23–40. Springer, 2024.
- [4] Qihao Liu, Xi Yin, Alan Yuille, Andrew Brown, and Mannat Singh. Flowing from words to pixels: A framework for cross-modality evolution. *arXiv preprint arXiv:2412.15213*, 2024.
- [5] Ju He, Qihang Yu, Qihao Liu, and Liang-Chieh Chen. Flowtok: Flowing seamlessly across text and image tokens. *arXiv preprint arXiv:2503.10772*, 2025.
- [6] Lvmin Zhang, Anyi Rao, and Maneesh Agrawala. Adding conditional control to text-to-image diffusion models. In *Proceedings of the IEEE/CVF international conference on computer vision*, pages 3836–3847, 2023.
- [7] Jonathan Ho, Tim Salimans, Alexey Gritsenko, William Chan, Mohammad Norouzi, and David J Fleet. Video diffusion models. *Advances in Neural Information Processing Systems*, 35:8633–8646, 2022.

- [8] Xin Li, Wenqing Chu, Ye Wu, Weihang Yuan, Fanglong Liu, Qi Zhang, Fu Li, Haocheng Feng, Errui Ding, and Jingdong Wang. Videogen: A reference-guided latent diffusion approach for high definition text-to-video generation. [arXiv preprint arXiv:2309.00398](#), 2023.
- [9] Yang Jin, Zhicheng Sun, Ningyuan Li, Kun Xu, Hao Jiang, Nan Zhuang, Quzhe Huang, Yang Song, Yadong Mu, and Zhouchen Lin. Pyramidal flow matching for efficient video generative modeling. [arXiv preprint arXiv:2410.05954](#), 2024.
- [10] Cheng Chi, Zhenjia Xu, Siyuan Feng, Eric Cousineau, Yilun Du, Benjamin Burchfiel, Russ Tedrake, and Shuran Song. Diffusion policy: Visuomotor policy learning via action diffusion. [The International Journal of Robotics Research](#), page 02783649241273668, 2023.
- [11] Allen Z Ren, Justin Lidard, Lars L Ankile, Anthony Simeonov, Pulkit Agrawal, Anirudha Majumdar, Benjamin Burchfiel, Hongkai Dai, and Max Simchowitz. Diffusion policy policy optimization. [arXiv preprint arXiv:2409.00588](#), 2024.
- [12] Dechen Gao, Hang Wang, Hanchu Zhou, Nejib Ammar, Shatadal Mishra, Ahmadreza Moradipari, Iman Soltani, and Junshan Zhang. In-ril: Interleaved reinforcement and imitation learning for policy fine-tuning. [arXiv preprint arXiv:2505.10442](#), 2025.
- [13] Yue Su, Xinyu Zhan, Hongjie Fang, Han Xue, Hao-Shu Fang, Yong-Lu Li, Cewu Lu, and Lixin Yang. Dense policy: Bidirectional autoregressive learning of actions. [arXiv preprint arXiv:2503.13217](#), 2025.
- [14] Qinglun Zhang, Zhen Liu, Haoqiang Fan, Guanghui Liu, Bing Zeng, and Shuaicheng Liu. Flowpolicy: Enabling fast and robust 3d flow-based policy via consistency flow matching for robot manipulation. In [Proceedings of the AAAI Conference on Artificial Intelligence](#), volume 39, pages 14754–14762, 2025.
- [15] Quentin Rouxel, Andrea Ferrari, Serena Ivaldi, and Jean-Baptiste Mouret. Flow matching imitation learning for multi-support manipulation. In [2024 IEEE-RAS 23rd International Conference on Humanoid Robots \(Humanoids\)](#), pages 528–535. IEEE, 2024.
- [16] Max Braun, Noémie Jaquier, Leonel Rozo, and Tamim Asfour. Riemannian flow matching policy for robot motion learning. In [2024 IEEE/RSJ International Conference on Intelligent Robots and Systems \(IROS\)](#), pages 5144–5151. IEEE, 2024.
- [17] Kevin Black, Noah Brown, Danny Driess, Adnan Esmail, Michael Equi, Chelsea Finn, Niccolo Fusai, Lachy Groom, Karol Hausman, Brian Ichter, et al. $\pi 0$: A vision-language-action flow model for general robot control, 2024. URL <https://arxiv.org/abs/2410.24164>.
- [18] Yaron Lipman, Ricky T. Q. Chen, Heli Ben-Hamu, Maximilian Nickel, and Matt Le. Flow matching for generative modeling, 2023.
- [19] Jascha Sohl-Dickstein, Eric Weiss, Niru Maheswaranathan, and Surya Ganguli. Deep unsupervised learning using nonequilibrium thermodynamics. In [International conference on machine learning](#), pages 2256–2265. pmlr, 2015.
- [20] Sudeep Dasari, Oier Mees, Sebastian Zhao, Mohan Kumar Srirama, and Sergey Levine. The ingredients for robotic diffusion transformers. [arXiv preprint arXiv:2410.10088](#), 2024.
- [21] Ian Chuang, Andrew Lee, Dechen Gao, M Naddaf-Sh, Iman Soltani, et al. Active vision might be all you need: Exploring active vision in bimanual robotic manipulation. [arXiv preprint arXiv:2409.17435](#), 2024.
- [22] Zipeng Fu, Tony Z Zhao, and Chelsea Finn. Mobile aloha: Learning bimanual mobile manipulation using low-cost whole-body teleoperation. In [8th Annual Conference on Robot Learning](#), 2024.
- [23] Tony Z Zhao, Jonathan Tompson, Danny Driess, Pete Florence, Kamyar Ghasemipour, Chelsea Finn, and Ayzaan Wahid. Aloha unleashed: A simple recipe for robot dexterity. [arXiv preprint arXiv:2410.13126](#), 2024.
- [24] Ajay Mandlekar, Danfei Xu, Josiah Wong, Soroush Nasiriany, Chen Wang, Rohun Kulkarni, Li Fei-Fei, Silvio Savarese, Yuke Zhu, and Roberto Martín-Martín. What matters in learning from offline human demonstrations for robot manipulation. In [Conference on Robot Learning \(CoRL\)](#), 2021.
- [25] Olaf Ronneberger, Philipp Fischer, and Thomas Brox. U-net: Convolutional networks for biomedical image segmentation. In [International Conference on Medical image computing and computer-assisted intervention](#), pages 234–241. Springer, 2015.
- [26] Tony Z Zhao, Vikash Kumar, Sergey Levine, and Chelsea Finn. Learning fine-grained bimanual manipulation with low-cost hardware. [arXiv preprint arXiv:2304.13705](#), 2023.
- [27] Andrew Lee, Ian Chuang, Ling-Yuan Chen, and Iman Soltani. Interact: Inter-dependency aware action chunking with hierarchical attention transformers for bimanual manipulation. [arXiv preprint arXiv:2409.07914](#), 2024.

- [28] Letian Fu, Huang Huang, Gaurav Datta, Lawrence Yunliang Chen, William Chung-Ho Panitch, Fangchen Liu, Hui Li, and Ken Goldberg. In-context imitation learning via next-token prediction. arXiv preprint arXiv:2408.15980, 2024.
- [29] Zhefei Gong, Pengxiang Ding, Shangke Lyu, Siteng Huang, Mingyang Sun, Wei Zhao, Zhaoxin Fan, and Donglin Wang. Carp: Visuomotor policy learning via coarse-to-fine autoregressive prediction. arXiv preprint arXiv:2412.06782, 2024.
- [30] Fan Zhang and Michael Gienger. Affordance-based robot manipulation with flow matching. arXiv preprint arXiv:2409.01083, 2024.
- [31] Ethan Perez, Florian Strub, Harm De Vries, Vincent Dumoulin, and Aaron Courville. Film: Visual reasoning with a general conditioning layer. In Proceedings of the AAAI conference on artificial intelligence, volume 32, 2018.
- [32] Alexander Tong, Nikolay Malkin, Kilian Fatras, Lazar Atanackovic, Yanlei Zhang, Guillaume Huguet, Guy Wolf, and Yoshua Bengio. Simulation-free schrödinger bridges via score and flow matching, 2024.
- [33] Michael S Albergo and Eric Vanden-Eijnden. Building normalizing flows with stochastic interpolants. arXiv preprint arXiv:2209.15571, 2022.
- [34] Alexander Tong, Nikolay Malkin, Kilian Fatras, Lazar Atanackovic, Yanlei Zhang, Guillaume Huguet, Guy Wolf, and Yoshua Bengio. Simulation-free schrödinger bridges via score and flow matching. arXiv preprint arXiv:2307.03672, 2023.
- [35] Xingchao Liu, Chengyue Gong, and Qiang Liu. Flow straight and fast: Learning to generate and transfer data with rectified flow. arXiv preprint arXiv:2209.03003, 2022.
- [36] Alexander Tong, Kilian Fatras, Nikolay Malkin, Guillaume Huguet, Yanlei Zhang, Jarrid Rector-Brooks, Guy Wolf, and Yoshua Bengio. Improving and generalizing flow-based generative models with minibatch optimal transport. arXiv preprint arXiv:2302.00482, 2023.
- [37] Kaiming He, Xiangyu Zhang, Shaoqing Ren, and Jian Sun. Deep residual learning for image recognition. In Proceedings of the IEEE conference on computer vision and pattern recognition, pages 770–778, 2016.
- [38] Remi Cadene, Simon Alibert, Alexander Soare, Quentin Gallouedec, Adil Zouitine, Steven Palma, Pepijn Kooijmans, Michel Aractingi, Mustafa Shukor, Dana Aubakirova, Martino Russi, Francesco Capuano, Caroline Pascal, Jade Choghari, Jess Moss, and Thomas Wolf. Lerobot: State-of-the-art machine learning for real-world robotics in pytorch. <https://github.com/huggingface/lerobot>, 2024.
- [39] Ashish Vaswani, Noam Shazeer, Niki Parmar, Jakob Uszkoreit, Llion Jones, Aidan N Gomez, Łukasz Kaiser, and Illia Polosukhin. Attention is all you need. Advances in neural information processing systems, 30, 2017.
- [40] Jonathan Ho, Ajay Jain, and Pieter Abbeel. Denoising diffusion probabilistic models. Advances in neural information processing systems, 33:6840–6851, 2020.
- [41] Xingchao Liu, Chengyue Gong, and Qiang Liu. Flow straight and fast: Learning to generate and transfer data with rectified flow, 2022.
- [42] Patrick Esser, Sumith Kulal, Andreas Blattmann, Rahim Entezari, Jonas Müller, Harry Saini, Yam Levi, Dominik Lorenz, Axel Sauer, Frederic Boesel, et al. Scaling rectified flow transformers for high-resolution image synthesis, 2024. URL <https://arxiv.org/abs/2403.03206>, 2.
- [43] Qihao Liu, Zhanpeng Zeng, Ju He, Qihang Yu, Xiaohui Shen, and Liang-Chieh Chen. Alleviating distortion in image generation via multi-resolution diffusion models and time-dependent layer normalization. Advances in Neural Information Processing Systems, 37:133879–133907, 2024.
- [44] Sucheng Ren, Qihang Yu, Ju He, Xiaohui Shen, Alan Yuille, and Liang-Chieh Chen. Flowar: Scale-wise autoregressive image generation meets flow matching. arXiv preprint arXiv:2412.15205, 2024.
- [45] Songming Liu, Lingxuan Wu, Bangguo Li, Hengkai Tan, Huayu Chen, Zhengyi Wang, Ke Xu, Hang Su, and Jun Zhu. Rdt-1b: a diffusion foundation model for bimanual manipulation. arXiv preprint arXiv:2410.07864, 2024.
- [46] Johannes S Fischer, Ming Gui, Pingchuan Ma, Nick Stracke, Stefan A Baumann, and Björn Ommer. Boosting latent diffusion with flow matching. arXiv preprint arXiv:2312.07360, 2023.
- [47] Xingchao Liu, Chengyue Gong, and Qiang Liu. Flow straight and fast: Learning to generate and transfer data with rectified flow. arXiv preprint arXiv:2209.03003, 2022.
- [48] Alec Radford, Jong Wook Kim, Chris Hallacy, Aditya Ramesh, Gabriel Goh, Sandhini Agarwal, Girish Sastry, Amanda Askell, Pamela Mishkin, Jack Clark, Gretchen Krueger, and Ilya Sutskever. Learning transferable visual models from natural language supervision. In Marina Meila and Tong Zhang, editors, Proceedings of the 38th International Conference on Machine Learning, volume 139 of Proceedings of Machine Learning Research, pages 8748–8763. PMLR, 18–24 Jul 2021.

- [49] Aäron van den Oord, Yazhe Li, and Oriol Vinyals. Representation learning with contrastive predictive coding. CoRR, abs/1807.03748, 2018.
- [50] Diederik P. Kingma and Max Welling. Auto-Encoding Variational Bayes. In 2nd International Conference on Learning Representations, ICLR 2014, Banff, AB, Canada, April 14-16, 2014, Conference Track Proceedings, 2014.

A Proof of FLD and FLC Equivalence

Preliminaries. All norms below are vector norms with induced operator norms. We use the ball $B(\mathbf{z}_1, r) = \{\mathbf{x} : \|\mathbf{x} - \mathbf{z}_1\| < r\}$. Assumption 1 in the main text holds throughout.

Lemma 1 (Local bi-Lipschitzness from Jacobian bounds). *For any $\hat{\mathbf{z}}_1 \in B(\mathbf{z}_1, r)$,*

$$m \|\hat{\mathbf{z}}_1 - \mathbf{z}_1\| \leq \|\mathcal{D}_a(\hat{\mathbf{z}}_1) - \mathcal{D}_a(\mathbf{z}_1)\| \leq L \|\hat{\mathbf{z}}_1 - \mathbf{z}_1\|.$$

Proof of Lemma 1. Let $\gamma(s) = \mathbf{z}_1 + s(\hat{\mathbf{z}}_1 - \mathbf{z}_1)$ for $s \in [0, 1]$. The mean-value integral formula gives

$$\mathcal{D}_a(\hat{\mathbf{z}}_1) - \mathcal{D}_a(\mathbf{z}_1) = \int_0^1 J_{\mathcal{D}_a}(\gamma(s)) (\hat{\mathbf{z}}_1 - \mathbf{z}_1) ds.$$

Taking norms and using, for any matrix J and vector $v \neq 0$, $\sigma_{\min}(J)\|v\| \leq \|Jv\| \leq \sigma_{\max}(J)\|v\|$, together with $m \leq \sigma_{\min}(J_{\mathcal{D}_a}(\gamma(s)))$ and $\sigma_{\max}(J_{\mathcal{D}_a}(\gamma(s))) \leq L$ for all s , yields the bounds.

Proof of Theorem 1. Add and subtract $\mathcal{D}_a(\mathbf{z}_1)$ and apply triangle/reverse-triangle inequalities:

$$\begin{aligned} \|\mathcal{D}_a(\hat{\mathbf{z}}_1) - A\| &\leq \|\mathcal{D}_a(\hat{\mathbf{z}}_1) - \mathcal{D}_a(\mathbf{z}_1)\| + \|\mathcal{D}_a(\mathbf{z}_1) - A\|, \\ \|\mathcal{D}_a(\hat{\mathbf{z}}_1) - A\| &\geq \|\mathcal{D}_a(\hat{\mathbf{z}}_1) - \mathcal{D}_a(\mathbf{z}_1)\| - \|\mathcal{D}_a(\mathbf{z}_1) - A\|. \end{aligned}$$

Invoke Lemma 1 and set $\varepsilon_{\text{AE}} = \|\mathcal{D}_a(\mathbf{z}_1) - A\|$ to obtain the two-sided inequality stated in Theorem 1. The minimizer claims follow immediately: if $\varepsilon_{\text{AE}} = 0$, both losses are minimized at $\hat{\mathbf{z}}_1 = \mathbf{z}_1$; otherwise any minimizer of FLD must satisfy $\|\hat{\mathbf{z}}_1 - \mathbf{z}_1\| \leq \varepsilon_{\text{AE}}/m$.

Corollary A.1 (squared-loss version). Assume $\varepsilon_{\text{AE}} = 0$. Then

$$m^2 \|\hat{\mathbf{z}}_1 - \mathbf{z}_1\|^2 \leq \|\mathcal{D}_a(\hat{\mathbf{z}}_1) - A\|^2 \leq L^2 \|\hat{\mathbf{z}}_1 - \mathbf{z}_1\|^2.$$

With $\varepsilon_{\text{AE}} = 0$, Lemma 1 gives $m\|\hat{\mathbf{z}}_1 - \mathbf{z}_1\| \leq \|\mathcal{D}_a(\hat{\mathbf{z}}_1) - \mathcal{D}_a(\mathbf{z}_1)\| \leq L\|\hat{\mathbf{z}}_1 - \mathbf{z}_1\|$. Since both sides are nonnegative, squaring preserves the inequalities. Thus the squared FLD objective is sandwiched between m^2 and L^2 times the squared FLC objective. Consequently, the map $\hat{\mathbf{z}}_1 \mapsto \|\mathcal{D}_a(\hat{\mathbf{z}}_1) - A\|_2^2$ is locally L^2 -smooth and m^2 -strongly convex along latent directions (intuitively, its curvature is controlled by $J_{\mathcal{D}_a}^\top J_{\mathcal{D}_a}$ whose eigenvalues lie in $[m^2, L^2]$).

Corollary A.2 (gradient scaling for squared losses). Let $J := J_{\mathcal{D}_a}(\hat{\mathbf{z}}_1)$ and assume $\varepsilon_{\text{AE}} = 0$. For the squared losses,

$$\nabla_{\hat{\mathbf{z}}_1} \mathcal{L}_{\text{FLD}}^{(2)} = 2J^\top(\mathcal{D}_a(\hat{\mathbf{z}}_1) - A), \quad \nabla_{\hat{\mathbf{z}}_1} \mathcal{L}_{\text{FLC}}^{(2)} = 2(\hat{\mathbf{z}}_1 - \mathbf{z}_1).$$

Then

$$m^2 \|\nabla \mathcal{L}_{\text{FLD}}^{(2)}\| \leq \|\nabla \mathcal{L}_{\text{FLD}}^{(2)}\| \leq L^2 \|\nabla \mathcal{L}_{\text{FLC}}^{(2)}\|.$$

Use $\|J^\top y\| \in [m\|y\|, L\|y\|]$ (by singular-value bounds) with $y = \mathcal{D}_a(\hat{\mathbf{z}}_1) - A = \mathcal{D}_a(\hat{\mathbf{z}}_1) - \mathcal{D}_a(\mathbf{z}_1)$, and Lemma 1 to get $m\|y\| \leq \|J^\top y\| \leq L\|y\|$ and $m\|\hat{\mathbf{z}}_1 - \mathbf{z}_1\| \leq \|y\| \leq L\|\hat{\mathbf{z}}_1 - \mathbf{z}_1\|$. Multiplying the bounds yields $m^2\|\hat{\mathbf{z}}_1 - \mathbf{z}_1\| \leq \|J^\top y\| \leq L^2\|\hat{\mathbf{z}}_1 - \mathbf{z}_1\|$. Since $\|\nabla \mathcal{L}_{\text{FLC}}^{(2)}\| = 2\|\hat{\mathbf{z}}_1 - \mathbf{z}_1\|$, this gives the stated inequality (up to the common factor 2). It follows that step-size sensitivity is governed by the squared condition number $(L/m)^2$.

B Extended Ablations

B.1 Dimensionality Matching for Vision-to-Action Flow

A constraint of flow matching is that the source and target must have identical shapes. In visuomotor contexts, the visual latent representations (\mathbf{z}_0) are typically much higher-dimensional than raw action chunks (A). A naive solution would be to down-sample the visual representation to match the action dimensionality, which, nevertheless, leads to significant information loss and poor performance, particularly when the dimensional gap is large.

Therefore, we adopt the opposite strategy: we map the raw action chunks into a higher-dimensional latent space that matches the dimensionality of the visual latent representations.

A naive approach is to use fixed linear transformations. When the action dimension is smaller than the latent dimension, we construct a lossless mapping by embedding the actions into the higher-dimensional latent space through zero-padding. The inverse mapping simply discards the padding. Our experiments show that action representations produced by such transformations are insufficient for learning reasonable flow matching policies. We found that learning well-structured action latent spaces via autoencoders as the target distributions for flow matching can be crucial for the success of vision-to-action flow. We develop an action encoder (\mathcal{E}_a), which does not simply remap dimensions, but also learns structured latent action spaces, making the complex flow from vision to action more tractable.

Table 4: Task SR (%) on ThreadNeedle with different action up-sampling strategies.

Up-sampling Strategy	SR (%)
Zero-Padding	0
Action AE (w/o FLD)	0
Action AE (w/ FLD)	92

Autoencoder Loss Selection. We utilize the L1 loss for the autoencoder loss, \mathcal{L}_{AE} . We found it outperforms the L2 loss, which is prone to mode-averaging and can result in blurry action reconstruction.

Sampling Stochasticity. We examined VITA variants with different sources of sampling stochasticity. We found that introducing dropout in the network, or variance (σ) in flow matching (where σ injects Gaussian noise into the interpolation path between source and target latents as in OT-CFM) degrades performance. In contrast, adding covariance to the source distribution yields results comparable to the deterministic implementation. Similarly, using a variational objective in the action autoencoder performs on par, whereas applying a variational objective to the image encoder significantly hurts performance (see Figure 11).

C Experiment Results

VITA exhibits efficient and stable learning on AV-ALOHA and PushT (Figure 8) and Robomimic tasks (Figure 9).

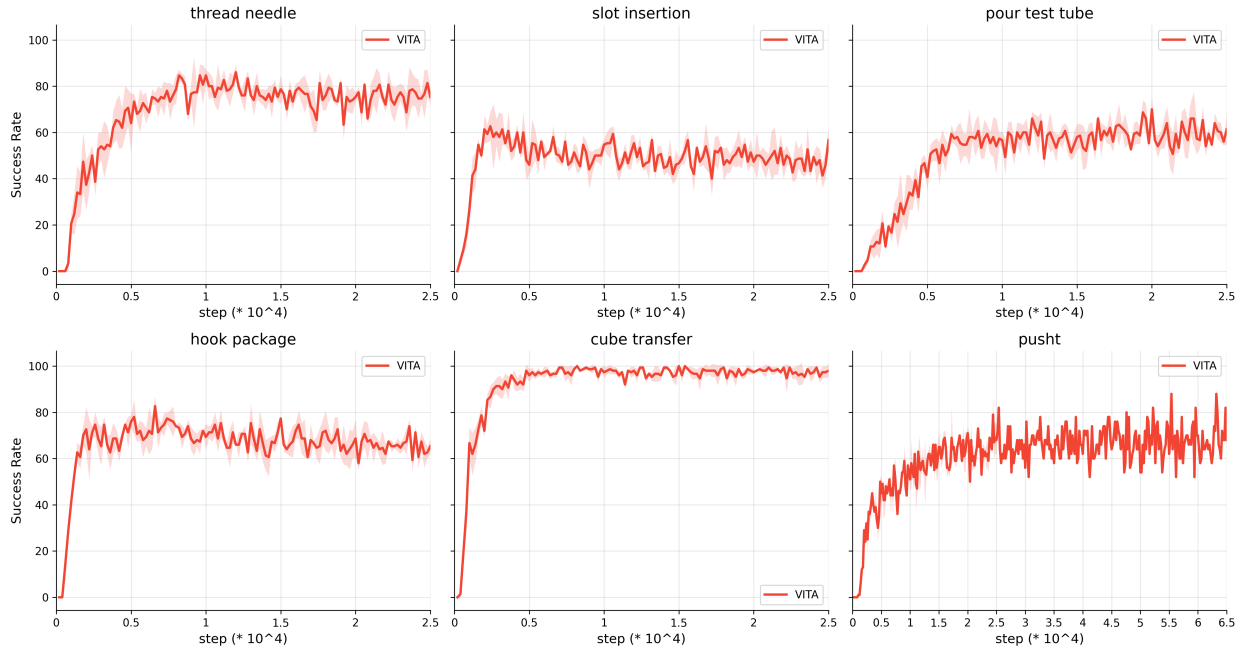


Figure 8: Success rate curves of VITA training on six tasks (five AV-ALOHA + PushT). The curves are mean across three random seeds; the shaded region is ± 1 standard deviation.

D Extended Related Works

Imitation Learning for Visuomotor Policy. Imitation learning enables robots to learn complex behaviors by mimicking expert demonstrations. Behavioral cloning, a prominent imitation learning paradigm, frames this as a supervised learning problem, learning a policy that maps observations to actions [26, 27]. Recent advancements in behavioral cloning have widely adopted two modeling methods: generative modeling and autoregressive modeling. Generative methods learn a conditional distribution of actions given an observation. This category includes policies based on conditional variational autoencoders (CVAEs) [26, 27], as well as diffusion [20, 10] and flow matching [30, 14].

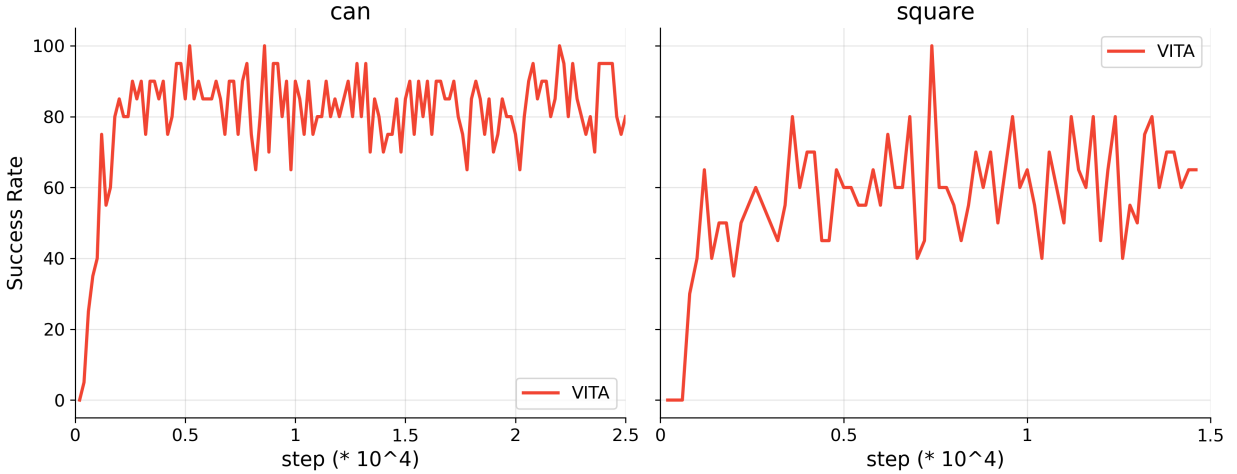


Figure 9: Success rate curves of VITA training on two Robomimic tasks.

On the other hand, autoregressive methods tokenize actions and frame policy learning as a sequence modeling task. These methods predict action tokens sequentially, using next-token prediction [28], next-scale prediction [29], or bi-directional prediction [13]. Generative models ubiquitously require extra conditioning modules (e.g., cross-attention [20], AdaLN [20], FiLM [31, 10]) to inject observations at each step of the generation process. Furthermore, generative and autoregressive methods commonly employ large, expressive networks such as U-Nets or transformers to succeed on complex, high-dimensional robotics tasks. VITA reduces these complexity by formulating the policy as a noise-free and conditioning-free vision-to-action flow; by using vector representations for vision and action, VITA also enables simple and lightweight MLP-only network for policy parameterization, even for challenging bi-manual manipulation tasks.

Diffusion and Flow matching for Generative Modeling. Diffusion [40], grounded in stochastic differential equations (SDEs), generates complex data distributions by sampling from a simple source distribution (typically Gaussian) and iteratively denoising it to the target distribution [19]. Flow matching [18, 41] has been proposed to enable faster training and sampling [41, 32, 42, 18] by modeling the map between source and target distributions with an ordinary differential equation (ODE). Both diffusion and flow matching models have shown strong performance across diverse generative tasks, such as image generation [1, 2, 3, 6, 43, 44], video generation [7, 8], and visuomotor policies [10, 20, 17, 45]. Unlike diffusion, flow matching theoretically places no constraints on the choice of source distribution [32], and a few works have explored leveraging this property to learn the direct transport within the same modality [33, 34], e.g., for image-to-image generation tasks [46, 47]. Recently, [4] and [5] extended this to more challenging cross-modal generation between text and image. VITA focuses on learning to bridge vision and action for visuomotor control, where the target modality, action, features sparser data, and lacks semantic structures, compared to text or images, presenting unique challenges. Different from flow matching for image generation, which typically pre-trains and freezes the image encoder and decoder when learning flow matching or diffusion models for image generation [1, 5, 4], VITA resorts to a fully end-to-end pipeline training to effectively learn the latent action space from limited and sparse action data. Furthermore, to enable effective joint training of flow matching and target latent spaces, we propose flow latent decoding to backpropagate action reconstruction losses through the the latent action generation process (ODE solving steps) during training.

E Discussion of Training Objectives

E.1 Contrastive Latent Alignment

Section 4.4 introduced two key objectives, FLD and its surrogate FLC, which are both designed to prevent latent space collapse and enable effective VITA learning. Empirically, we find that FLD alone outperforms FLC alone, as it provides a more direct training signal by anchoring the generation process to the ground-truth actions. However, the most robust performance is achieved by combining them, which enforces consistency in both latent space and action space.

Additionally, motivated by the ability of contrastive learning to improve representations and prevent latent collapse [4], we introduced a contrastive loss between vision and action latents [48]. We show that this objective can further boost

performance beyond FLD and FLC on some tasks by encouraging the model to learn representations where the similarity between corresponding vision-action pairs is maximized, while the similarity between non-corresponding pairs is minimized.

We employ InfoNCE (Noise-Contrastive Estimation) [49] for contrastive learning between vision and action. For a given batch of size N , the vision latent $z_{0,i}$ and action latent $z_{1,i}$ from the same data sample are treated as a positive pair. All other non-corresponding combinations $(z_{0,i}, z_{1,j})$ where $i \neq j$ are considered negative pairs. The loss aims to maximize the similarity of positive pairs while minimizing the similarity of negative pairs. The symmetric InfoNCE loss is defined as:

$$\mathcal{L}_{\text{contrastive}} = -\frac{1}{2N} \sum_{i=1}^N \left[\log \frac{\exp(\text{sim}(z_{0,i}, z_{1,i})/\tau)}{\sum_{j=1}^N \exp(\text{sim}(z_{0,i}, z_{1,j})/\tau)} + \log \frac{\exp(\text{sim}(z_{1,i}, z_{0,i})/\tau)}{\sum_{j=1}^N \exp(\text{sim}(z_{1,i}, z_{0,j})/\tau)} \right]$$

where $\text{sim}(\cdot, \cdot)$ denotes the cosine similarity between L2-normalized feature vectors and τ is a temperature hyperparameter.

As shown in Figure 10, the contrastive objective, when used alone, is insufficient for effective VITA learning and underperforms VITA with only the FLD loss (see Figure 6). However, it provides additional performance gains when combined with the FLD and FLC losses, as it helps create a more robust and well-structured latent space.

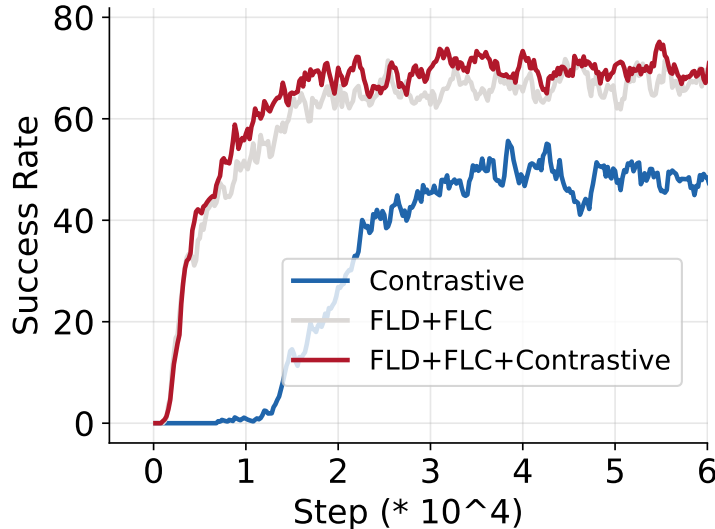


Figure 10: Success rates using different VITA learning objectives with or without contrastive losses.

E.2 Ablation of the Action Autoencoder

In our experiments, a deterministic autoencoder (AE) learns the target latent space for actions. To investigate the effect of imposing a prior on this latent space, we conducted an ablation study replacing the AE with a variational autoencoder (VAE) [50]. This change introduces a KL divergence regularization term, weighted by λ_{KL} , which encourages the encoder’s posterior output, $q(z_1 | A)$, to match a standard normal prior:

$$\mathcal{L}_{\text{KL}} = D_{\text{KL}}(q(z_1 | A) || p(z_1)), \quad p(z_1) = \mathcal{N}(0, I).$$

As shown by the training curves in Figure 11(a) and Figure 12, incorporating this variational objective with various weights (λ_{KL}) can degrade model performance.

E.3 Ablation of the Vision Encoder

As described in our main architecture (Figure 2), the source latent variable $z_0 = \mathcal{E}_v(O) \in \mathbb{R}^{D_{\text{latent}}}$ is produced by a deterministic vision encoder. We performed a similar ablation to assess the impact of a prior on this visual latent

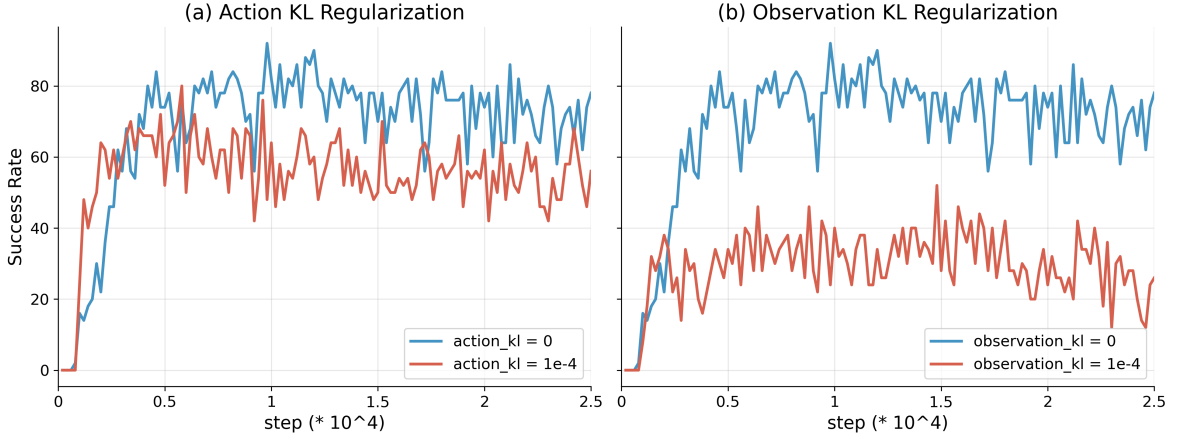


Figure 11: Ablation of VAE for action (a) and vision (b) on ThreadNeedle.

space. Specifically, we replaced the deterministic encoder with a variational one that models the posterior $q(z_0 | O)$ and introduces a corresponding KL divergence loss (weighted by $\lambda_{\text{KL}}^{\text{obs}}$):

$$\mathcal{L}_{\text{KL}}^{\text{obs}} = D_{\text{KL}}(q(z_0 | O) \parallel p(z_0)), \quad p(z_0) = \mathcal{N}(0, I).$$

As shown in Figure 11(b), using a VAE for the vision encoder drastically degrades performance.

F Task Settings

Dataset	State Dim	Action Dim	FPS	Image Size	Camera
AV-ALOHA (Sim)	21	21	8.33	240×320	zed_cam_left
AV-ALOHA (Real)	21	21	11	240×320	left_eye_cam
RoboMimic	43	7	20	256×256	agentview_image

Table 5: Comparison of dataset specifications.

F.1 AV-ALOHA Simulation tasks.

CubeTransfer: Pick up a red cube with the right arm and transfer it to the left arm (200 episodes).

SlotInsertion: Use both arms to pick up a green stick and insert it into a pink slot (100 episodes).

HookPackage: Use both arms to pick up a red box and hook it onto a blue wall-mounted hook (100 episodes).

PourTestTube: Pick up two test tubes and pour a small red ball from one into the other (100 episodes).

ThreadNeedle: Pick up a green needle and thread it through the hole of a pink object (200 episodes).

F.2 AV-ALOHA Real tasks

HiddenPick: Lift and open a fabric cover from a box, then pick an object from inside (50 episodes).

TransferFromBox: Pick an object from a box with the right arm, transfer it to the left arm, and place it in another box (50 episodes).

F.3 Robomimic Tasks

Robomimic is a benchmark of single-arm imitation learning tasks [24]. We adapt the environment for compatibility with the LeRobot [38] codebase. The robot state includes arm joint positions (encoded with sin and cos), joint velocities, end-effector pose, gripper finger positions, and gripper finger velocities. The action space consists of six values for delta position control of the end-effector pose and one value for the absolute position of the gripper.

Square: Pick up a square nut and insert it onto a matching square peg (175 episodes).

Can: Pick up a red can and place it into a box (192 episodes).

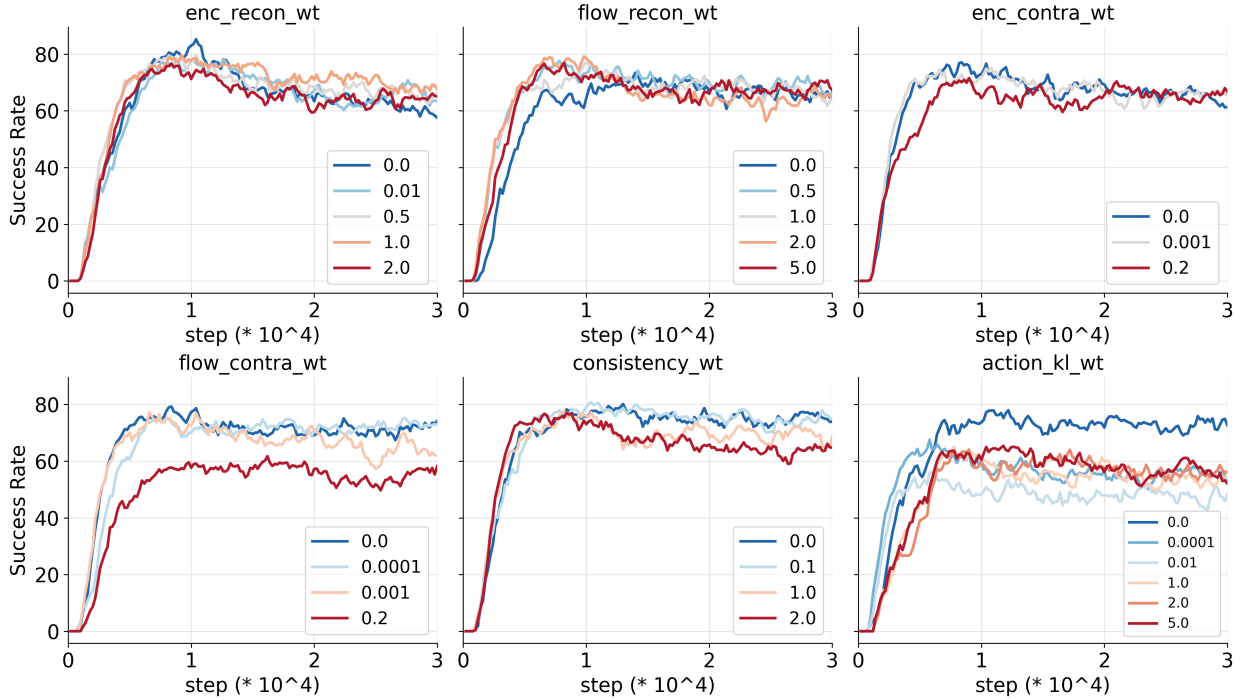


Figure 12: Hyperparameter ablations on ThreadNeedle. Each sub-plot varies a single coefficient while holding all others at their default values in Table 6. Top: action encoder reconstruction weight, flow latent decoding weight, action encoder contrastive weight. Bottom: latent flow contrastive weight, latent flow consistency weight, action KL weight.

G Training

In each plot of Figure 12, we sweep a single weight while holding all other hyperparameters at the default (Table 6), and visualize the success rates over training steps. With these experimental results, a robust configuration on ThreadNeedle includes moderate weights for both AE and FLD (typically in $[0.5, 1.0]$), moderate FLC, minimal or no contrastive penalties, and no KL regularization on the action and vision latent.

H Implementations

H.1 VITA

VITA encodes observations into a latent vector z_0 using a ResNet-18 backbone. The flow network, which learns the mapping from z_0 to \hat{z}_1 , is implemented as an MLP. We use a 6-step Euler ODE solver. The latent action \hat{z}_1 is translated to action chunks by a lightweight MLP-based action decoder. A summary of all hyperparameters and loss weights is provided in Table 6.

H.2 Flow Matching Policy

The FM policy learns a velocity field using a transformer backbone, with AdaLN for conditioning. A 6-step Euler solver is used for solving ODEs. The hyperparameters and loss weights are summarized in Table 7.

Table 6: VITA hyperparameters.

Horizons & Observation	
Observation horizon	1
Prediction horizon	16
Action horizon	8
Observer backbone	resnet18
Observer tokenize	false
VITA core (latent & losses)	
Latent dimension (D_{latent})	512
Decode flow latents	true
Consistency weight	1.0
Encoder contrastive weight	1e-4
Flow contrastive weight	0.0
Latent noise std	0.0
Flow matcher / ODE	
Flow Matcher	OT-CFM
σ	0.0
# sampling steps (Euler)	6
Action AE	
AE recon loss type	l1
Encoder recon weight	0.5
Flow recon (FLD) weight	0.5
Use variational (VAE)	false
KL weight (if variational)	1e-6
Freeze encoder / decoder	false / false
Pretrained path	None
AE network (encoder/decoder)	
Encoder type / hidden dim	cnn / 512
Decoder type / hidden dim	simple / 512
Latent dim (AE)	512
Num heads / MLP ratio	8 / 4
Dropout	0.0
Num layers	4

H.3 Diffusion Policy

We follow the DP [10] implementation in LeRobot [38]. The core of the policy is a U-Net noise predictor, which uses FiLM [31] for conditioning. The model is trained for 100 timesteps using a cosine beta schedule. During inference, trajectories are generated using a 10-step DDPM sampler. All hyperparameters and loss weights are listed in Table 8.

H.4 Action Chunking Transformer

We follow the ACT [26] implementation in LeRobot [38]. ACT is a conditional variational autoencoder (cVAE) that generates action chunks conditioned on vision. Its architecture consists of a vision encoder for processing observations and a transformer-based decoder that models the distribution of future actions conditioned on the visual input. A complete list of hyperparameters and loss weights is provided in Table 9.

Table 7: **Flow Matching (FM) Policy hyperparameters.**

Horizons & Observation	
Observation horizon	1
Prediction horizon	16
Action horizon	8
Observer backbone	resnet18
Observer tokenize	false
Flow matcher / ODE	
Flow Matcher	Target
σ	0.0
# sampling steps	6
Flow network architecture	
Backbone	flow_transformer
Conditioning	adaln (<i>options: adaln, cross, cross_adaln</i>)
Hidden dim	512
Num layers	4
Num heads	8
MLP ratio	4
Dropout	0.1

Table 8: **Diffusion policy hyperparameters.**

Horizons & Observation	
Observation horizon	1
Prediction horizon	16
Action horizon	8
Observer backbone	resnet18
Observer tokenize	false
Mask loss for padding	false
Diffusion scheduler	
Type	DDPM
Training timesteps	100
Beta schedule	squaredcos_cap_v2
Beta start / end	1e-4 / 2e-2
Prediction type	epsilon
Clip sample / range	true / 1.0
U-Net architecture	
Down dims	[512, 1024, 2048] or [256,512,1024]
Kernel size	5
Group norm groups	8
Diffusion step embed dim	128
FiLM scale modulation	true
Optimization	
Adam LR / backbone scale	1e-4 / 0.1
Adam betas / eps	(0.95, 0.999) / 1e-8
Weight decay	1e-6
Scheduler	cosine, warmup 500 steps
Training & inference	
Total training steps	200000
Inference steps	null (defaults to training timesteps)

Table 9: Action Chunking Transformer (ACT): hyperparameters.

Sequence horizons	
Action horizon	8
Prediction horizon	16
Observation horizon	1
Observer / backbone	
Image encoder	ResNet-18
Tokenize	false
Transformer (policy head)	
Pre-norm	false
Model dimension d_{model}	512
Attention heads	8
Feedforward dim	3200
FFN activation	ReLU
Encoder layers	4
Decoder layers	1
Dropout	0.1
Latent / VAE block	
Use VAE	true
Latent dim	32
VAE encoder layers	4
ACT KL weight	10.0
Optimization	
Optimizer	Adam
Learning rate	1×10^{-5}
Betas	(0.9, 0.999)
ϵ	1×10^{-8}
Weight decay	1×10^{-4}
Backbone LR scale	0.1
LR scheduler & validation	
Scheduler	Cosine
Warmup steps	2000
Online validation frequency	2000 steps